X mode Doppler Reflectometry k-spectral measurements in ASDEX Upgrade: Experiments and simulations

C.Lechte[1], G.D.Conway[2], T.Görler[2], C.Tröster-Schmid[2], and the ASDEX Upgrade Team

[1]Institut für Grenzflächenverfahrenstechnik und Plasmatechnologie IGVP, 70569 Stuttgart, Germany

[2]Max-Planck-Institut für Plasmaphysik, Boltzmannstr. 2, 85748 Garching, Germany

Abstract.

The perpendicular density fluctuation spectrum in the tokamak ASDEX Upgrade was measured with Doppler reflectometry. In this paper, extensive plasma turbulence and microwave propagation simulations with the GENE gyro-kinetic code and the IPF-FD3D full-wave code were undertaken to explain the observed spectral shape. It was shown that in this case the X-mode polarization suffers both from a large non-linear saturation effect at low-to-intermediate probed wavenumbers, and a super-linear enhancement effect at large wavenumbers. With these effects, we were able to explain the observed discrepancies between the GENE perpendicular wavenumber spectra and the Doppler reflectometry derived wavenumber spectra. While the agreement is not perfect, the simulations give guidance on how to interpret X-mode Doppler reflectometry spectra.

PACS numbers: 52.35.Ra, 52.25.Fi, 52.55.-s, 52.70.-m, 52.65.Tt, 52.35.Hr

Submitted to: *PPCF*
Draft: 12 June 2017

1. Introduction

In fusion plasmas there usually exists a broad wavenumber spectrum $S(k)$ of density fluctuations that are responsible for radial transport and therefore losses. These range from low perpendicular wavenumbers $k_\perp$ (ion gyroradius scales) ion temperature gradient driven (ITG) modes to high $k_\perp$ (electron gyroradius scales) electron temperature gradient driven (ETG) modes. Since material probes cannot be employed in the plasma confinement region – the radial region of interest (up to normalized poloidal flux radius $0.5 < \rho_{\mathrm{pol}} < 1.0$), a contact-less diagnostic has to be used, such as spectroscopic, beam emission diagnostics, and microwave based techniques.

Microwave reflectometry is such a diagnostic which can measure the electron density profile, density fluctuations and plasma flows [1]. An incident microwave beam is reflected at a cutoff layer in the plasma and the reflected or scattered radiation is detected. Reflectometry is routinely used as a density profile diagnostic in fusion experiments [2], where a beam of increasing frequency is reflected by cutoff layers that are successively further inside the plasma. Reflectometry is also sensitive to density fluctuations. Since turbulence phenomena and the related radial transport are one of the major problems of magnetically confined fusion research, it is therefore important to have density fluctuation diagnostics that are both temporally, spatially and wavenumber resolved.

There are two possible setups for reflectometry. In conventional reflectometry, the incident wave vector is perpendicular to the cut-off layer, and the receiver looks at the $m = 0$ reflection order. This configuration is used for density profile measurements.

In Doppler reflectometry [3, 4, 5], the receiving antenna is tilted relative to the cutoff. Figure 1 shows the experimental setup [6, 7] in ASDEX Upgrade (AUG) – major radius $R = 1.6\,\mathrm{m}$ and minor radius $a = 0.5\,\mathrm{m}$ horizontally and $b = 0.8\,\mathrm{m}$ vertically, and a typical toroidal magnetic field of 2.5 T. The non-normal incidence causes a Doppler shift of the moving scattered wave, allowing the determination of the perpendicular velocity $v_\perp$ of the cutoff layer perturbations. Doppler reflectometry is well established as a robust $v_\perp$ diagnostic (cf. in AUG [7, 9]). However, the scattering sensitivity changes with the probed wavenumber and must be determined independently of the experiment.

This paper concentrates on the shape of the wavenumber spectrum and its modification by the scattering diagnostic. Experimental Doppler spectra and density spectra from turbulence simulations show marked differences in the position and shape of the inertial range of the turbulence. In addition, X mode Doppler measurements have been found to disagree with laser scattering and O mode Doppler measurements on Tore Supra [8]. Fullwave simulations with the IPF-FD3D code using realistic turbulence data generated by the GENE plasma turbulence code show how the spectrum produced by the diagnostic differs from the underlying density fluctuation spectrum. The modelling of the reflectometry response using full-wave codes and simulated turbulence is an active field and several preliminary approaches have been made [10, 11, 12] and [13] (analytic fluctuations only).

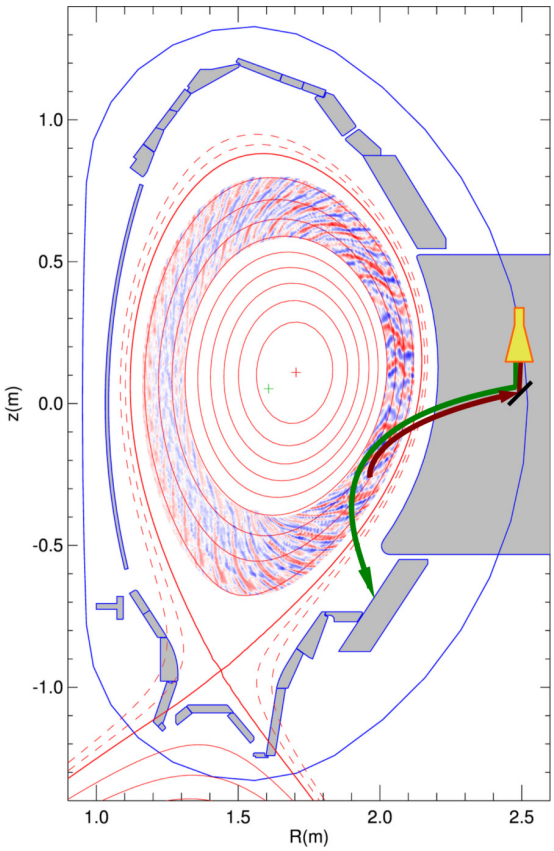

Figure 1. (Colour Online): Poloidal cross section of AUG with flux surfaces (for shot 22009) in red, with overlayed density fluctuation field from numerical simulations. The reflectometry antennas (at $R = 2.407\,\mathrm{m}$ and $z = 0.043\,\mathrm{m}$) are shown to the right, with an emitted and a back-scattered ray.

In the next section, the Doppler reflectometry principle is introduced, followed by a description of the experimental Doppler diagnostic on AUG used in this work, then the turbulence code GENE, which is used to generate the numerical turbulence data tailored to the experimental discharge, and then the full-wave code IPF-FD3D, which is used to simulate the Doppler diagnostic using the turbulent plasma simulations given by GENE. Finally, results from the full-wave simulations and conclusions are reported.

2. Doppler reflectometry

Doppler reflectometry (also called Doppler backscatter) is a hybrid technique combining the radial localization of reflectometry with the wavenumber sensitivity of coherent scattering. The usual implementation involves a microwave beam being launched into the plasma such that it approaches the cutoff layer obliquely and is turned and reflected away. Here, the beam turning point is where the refractive index N along the beam path reaches a minimum. If there are turbulent refractive index fluctuations around the beam turning point which satisfy the Bragg condition, then part of the incident beam

will be back-scattered to the reflectometer receiving antenna. For a monostatic antenna configuration (same antenna for launching and receiving, e.g. $m = -1$ Bragg order) the Bragg condition is:

$$\vec{k}_{fluct} = -2\vec{k}_i = -2\vec{N}k_o \tag{1}$$

where $\vec{k}_{fluct}$ is the probed density fluctuation wavenumber, $\vec{k}_i$ the incident beam wavevector at the turning point and k_o the microwave vacuum wavenumber. For a slab geometry, i.e. flat refractive index layers, $N = \sin\theta$ where θ is the angle between the incident wave and the flux surface normal. However, for the general case of curved flux/refractive index surfaces it is more usual to use ray or beam tracing techniques to determine $N^2 = N_\perp^2 + N_\parallel^2$ [6]. At the turning point the beam $k_r \to 0$. Likewise the turbulence $k_\parallel$ is small such that $k_\perp = -2N_\perp k_o$ dominates the back-scattered signal. To measure the fluctuation perpendicular wavenumber spectrum the reflectometer antenna tilt angle is varied to scan a range of wavenumbers.

Since the fluctuations are generally moving the received beam is also Doppler frequency shifted:

$$\omega_D = \vec{k} \cdot \vec{v} = -2k_o N_\perp v_\perp \tag{2}$$

where $v_\perp = v_{E\times B} + v_{ph}$ is the fluctuation velocity in the stationary laboratory measurement frame, i.e. the plasma $E_r \times B$ velocity plus the turbulence phase velocity. Usually the $E \times B$ drift dominates such that $v_\perp$ is therefore a measure of the radial electric field.

In the experiment, a number of significant complications arise when one wishes to recover the original fluctuation spectrum and its absolute amplitude from the Doppler signals. In a fusion plasma the fully developed turbulence is broadband with many different fluctuation wavenumbers present. Depending on the directivity of the receiving antenna, neighbouring wavenumbers with their corresponding Doppler shifts are also detected, leading to a finite width of the Doppler/wavenumber spectrum ($\Delta k/k \approx 0.2$–0.5 in simulations [10, 14]). In addition, higher-order m returns from harmonics of the nominally probed wavenumber appear at the same Doppler shift frequency and are indistinguishable from returns of the nominal wavenumber [4], albeit at low efficiency ($P \propto 1/m^2$).

Further difficulties arise in the presence of high ($> 5\,\%$) fluctuation levels, where the WKB or Born approximation [15] for modelling the scattering process breaks down. Here the signal will depend non-linearly on the fluctuation amplitude. The relationships given above are essentially valid only for single backscattering events – at high fluctuation amplitudes, multiple scattering can occur. In addition, the backscattering volume is not strictly localized to the beam turning point, so that the radial wavenumber spectrum of the fluctuations can also play a role in determining the received signal.

Some of these difficulties, like the localization of the beam turning point, can be surmounted using beam tracing techniques, which is done routinely as part of the data analysis process in AUG [6]. However, in general a 2D full-wave analysis is necessary to establish a particular reflectometer's *instrument response function* (ie. the

scattering efficiency), which would allow the recovery of the fluctuation spectra from the Doppler signal. The scattering efficiency is defined as the ratio of the received to the transmitted amplitude, normalized by the plasma density fluctuation strength parameter $Scat = (P_r/P_t)/\delta n$.

There are several methods that can be used to simulate the wave propagation in plasmas [16, 17, 18, 19, 20]. Of these, the finite-difference time domain method was chosen since it can handle arbitrary fluctuation strengths.

While there are many degrees of freedom in a fluctuation spectrum, there are two parameters that are typically used to describe a turbulence spectral shape, a transition wavenumber k_n, below which the spectrum is approximately flat, and an exponent α that describes the decay of the spectrum for $S(k_\perp > k_n) \propto k_\perp^\alpha$. Typical numbers for α, also called the *spectral index*, are $-5/3$ and -3 for three- and two-dimensional neutral fluid turbulence [21, 22]. For plasma turbulence, measured values for α range from -2 to -7. Different plasma operating regimes in fusion experiments are often characterized by changes in α. An alternative classification using exponentials was reported in [8], but is not used here.

3. Experimental measurements

3.1. Diagnostic setup

At this time, the Doppler reflectometer suite on AUG [6] consisted of two reflectometers in V-band ($52-74$ GHz) for X and O-mode probing respectively, with fixed tilt bistatic hog-horn antennas optimized for probing the edge plasma [7]; plus one reflectometer in W-band ($75-105$ GHz) with switchable O or X-mode and more core optimized antennas with a steerable tilt mirror [23, 24].

The measurements presented here used the W-band system with the steerable mirror. Figure 2 shows a schematic of the in-vessel antenna system, which consists of two folded hog-horn 30 dB gain antennas with ellipsoidal focusing mirrors. The two horns are radially adjacent and point vertically downward onto a plane mirror which is mechanically steerable in the poloidal plane with an angle span of $16^\circ > \theta_0 > -14^\circ$ relative to the horizontal, where negative angles point upwards. This results in two vertically separated beams but which are close enough together to constitute a single monostatic configuration.

The horns have approximately a Gaussian beam profile with a far-field 3 dB power half-width of 2.7° at 105 GHz in both horizontal and vertical E-planes. The mirror pivot point is situated near the equatorial $z = 0$ plane, which is generally some 20 cm below the magnetic equilibrium axis. The horns are fed directly by oversized 9×9 mm square waveguide (required to negotiate around the edge of the vacuum vessel port) then linear transitions to oversized 38 mm diameter circular smooth bore waveguide. The vacuum breaks consist of a pair of Gaussian periscopes with 10° tilted quartz windows. The ex-vessel oversized guides are some 6 m long. They terminate with linear tapers

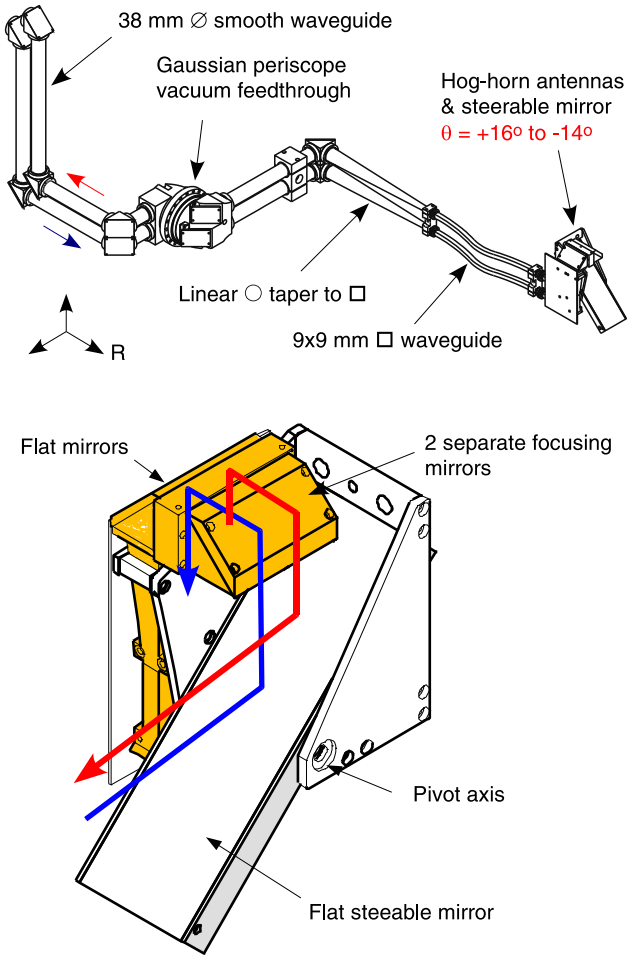

Figure 2. Schematic of the AUG Doppler reflectometer antenna layout. Top: waveguide transmission line routing, Bottom: Close-up of folded hog-horn antennas with steerable mirror.

to circular CR-10 and then transitions to rectangular fundamental WR-10 waveguide. The one-way loss is of the order of 6-8 dB. It should be noted that the antenna system has subsequently been removed and the waveguide feeds are now used for a bistatic Ultra-fast-swept profile reflectometer.

The reflectometer microwave circuit is shown schematically in figure 3 [23]. The transmit section consists of a $12-18$ GHz hyper-abrupt varactor tuned oscillator (HTO) phased locked via a stable 15 GHz dielectric resonator oscillator (DRO) and a phase comparator with programmable feedback N divider and a 900 MHz synthesized reference frequency. This section (shown as a yellow block) essentially forms a wide-band programmable microwave frequency synthesizer. The final launch frequency of $72-105$ GHz is obtained with a hextupler frequency multiplier and power amplifiers.

The heterodyne receiver is based on a fundamental mixer with a local oscillator (LO) reference generated by a second HTO2 and hextupler chain, locked to the launch oscillator HTO1 via a second phase-locked loop based on the 150 MHz HTO difference frequency. The resulting down-converted receiver mixer signal is finally detected using

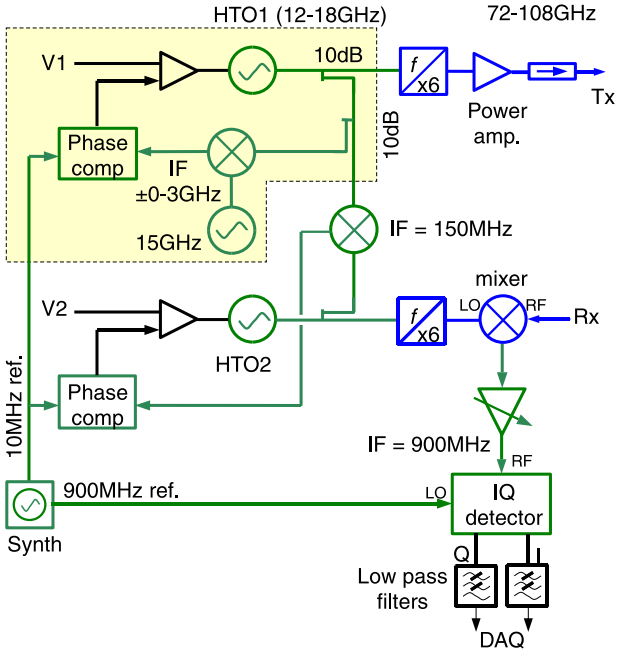

Figure 3. Schematic of the AUG Doppler reflectometer backend.

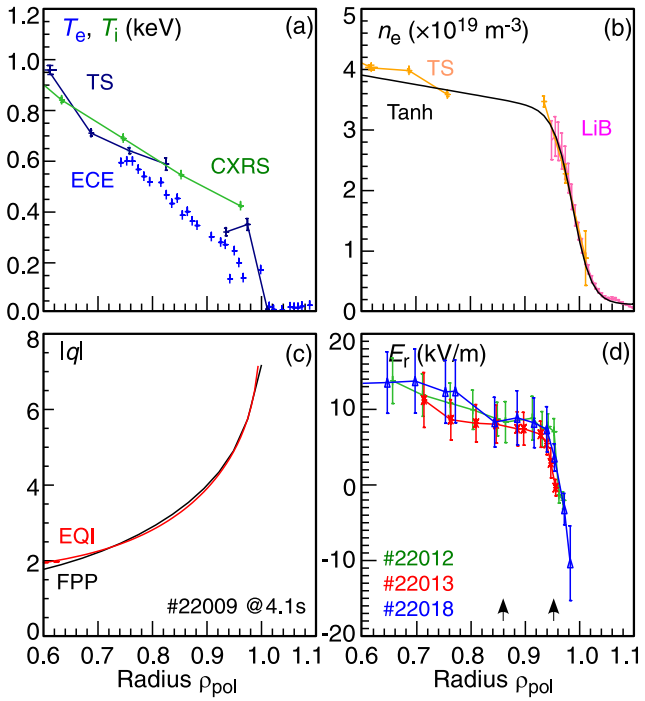

Figure 4. Experimental L-mode radial profiles for (a) T_e and T_i, (b) n_e (the solid black line is a Tanh fit) (c) safety factor $-q$ for AUG shot #22009, and (d) E_r for shots #22012, 22013 and 22018 with varying antenna tilts.

a 900 MHz In-phase and Quadrature (IQ) detector circuit and low-pass filters. The I and Q signals are digitized at 20 MHz in 12-bit resolution.

Since both the launch power and the receiver mixer sensitivity vary with the probing frequency it is necessary to calibrate the diagnostic power response. This was obtained by connecting the transmitter, via an attenuator, to the receiver and recording the IF signal power as a function of frequency. Across the W-band the maximum variation was of the order of 10 dB.

3.2. Plasma measurements

The k-spectral measurements were made in a sequence of seven identical $B_{\rm t} = -2.5$ T, $I_{\rm p} = +0.8$ MA lower-single-null discharges during L-mode phases with 2.5 MW of neutral beam (NBI) heating. The core line-averaged density was a constant $n_{\rm eo} = 4.8{\times}10^{19}$ m^{-3}, $q_{95} \sim 5.6$ and stored energy $W_{\rm mhd} = 0.25$ MJ, and no MHD activity. Figure 4 shows edge kinetic profiles of (a) $T_{\rm e}$ (ECE and Thomson Scattering) and $T_{\rm i}$ (CXRS), (b) $n_{\rm e}$ (TS, Li-beam), (c) the safety factor q (flux parameterized fit and CLISTE equilibrium reconstruction) for representative shot #22009, and (d) the $E_{\rm r}$ for shots #22012, 22013 and 22018 at 4.1 s. The solid-line in the density plot is a fitted Tanh profile to the Li-beam, TS and DCN interferometer data. This Tanh profile is used by both the TORBEAM and the full-wave simulations as input, as is the experimental equilibrium from the CLISTE reconstruction code. The fit function of the modified hyperbolic tangent is $c_0 + c_1\rho_{\rm pol} + c_2\tanh(c_3\rho_{\rm pol})$ with fit parameters c_i.

The mirror tilt angle was varied from shot-to-shot between $\theta_o = -2.3°$, $1.8°$, $6.5°$, $9.0°$, $11.5°$, $14.6°$ and $-12.4°$. During each shot the Doppler reflectometer probing frequency was stepped between 70.0 and 106.4 GHz in 22 non-uniform steps in a repeated sequence of 100 ms. TORBEAM beam tracing runs were performed for each antenna tilt angle and probing frequency combination to give a matrix of probed $k_\perp$ and measurement location $\rho_{\rm pol}$.

The concurrence of the $E_{\rm r}$ profiles in figure 4(d) for #22012 ($\theta_o = 9.0°$, $k_\perp \sim 10-13$ cm^{-1}), #22013 ($\theta_o = 11.5°$, $k_\perp \sim 13-15$ cm^{-1}) and #22018 ($\theta_o = -12.4°$, $k_\perp \sim 5-12$ cm^{-1}) confirms the general independence of the Doppler reflectometer $v_\perp$ measurement on the probed $k_\perp$.

Figure 5 shows X-mode Doppler spectra for a probing frequency of 93.3 GHz for shots #22012 (red: $\theta_o = +9.0°$) and #22018 (blue: $\theta_o = -12.4°$). The Doppler peak is obtained by fitting a Gaussian to the asymmetric component of the spectra (cf. [6]). The spectral power density $S(k_\perp) \propto |\tilde{n}(k_\perp)|^2 \propto A_D.w_D$ for the mean probed $k_\perp$ is then obtained by integrating the Gaussian fitted curve. No $k_\perp$ dependent calibration function is applied when presenting the experimental data.

Figure 6 shows the corresponding TORBEAM traces in the poloidal $[z:x]$ plane and toroidal $[y:x]$ plane for the two cases shown in figure 5. The x coordinate is the radial from the machine centre (major radius) to the antenna location. Since the antenna is aligned parallel to the side of the vacuum vessel port this results in a suboptimal $6.2°$

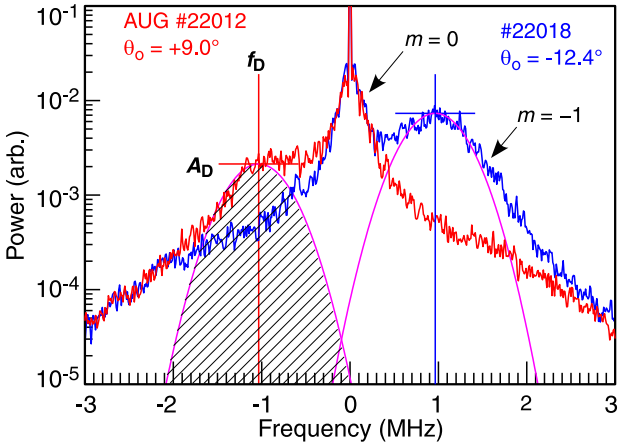

Figure 5. Doppler spectra at 93.3 GHz AUG shot #22012 (red: $\theta_o = +9.0°$) and #22018 (blue: $\theta_o = -12.4°$).

toroidal misalignment to the radial - which reduces somewhat the backscattered power. As can be seen, the antenna tilt scan can result in a substantial movement in the poloidal location of the sampling volume. The contour plot of GENE numerical turbulence in figure 1 suggests that there could potentially be a significant change in both the radial and poloidal turbulence structure, and the turbulent eddy alignment, over the vertical region scanned. Such a poloidal dependence on the turbulence structure would be more pronounced for smaller plasma minor radii. Nevertheless, both the experimental and the synthetic diagnostics will sample the local $k_\perp$, and hence for comparative purposes (code/diagnostic validation) should not have a detrimental effect. However, the impact of poloidal variations in the local $k_\perp$ could essentially distort the overall measured $S(k_\perp)$ spectra in an, as yet, unknown way, again complicating its interpretation.

The $S(k_\perp)$ spectra were built by taking two radial slices through the measurement matrix at $\rho_{\rm pol} \approx 0.85$ and 0.96 (corresponding to just inside and just outside the density pedestal location) as marked by arrows in figure 4(d). The measured spectral powers from the Gaussian fits are corrected for IF amplifier gains and the diagnostic power response. Figure 7 shows the resulting $k_\perp$ spectra. A constant waveguide attenuation is assumed for all frequencies (± 1 dB variations are incorporated into the spectral power error bars). The errors in $k_\perp$ are estimated from the Δk derived from the reflectometer beam spot size and flux surface curvature [5]. As can be seen, the spectra above $k_\perp \sim 5 - 6$ cm^{-1} decay with a constant spectral index of $\alpha \sim -3.8$. The points around $k_\perp \sim 5$ ($\theta_o = -12.4°$) suggest a roll over of the spectra, which appears to be supported by the points for $k_\perp < 2$ cm^{-1}, however, these data were acquired for a very shallow incident angle of $\theta_o = -2.3°$ and should be treated with some caution as there may be a degree of spectral contamination from the $m = 0$ component.

The spectral index of $\alpha = -3.8$ is supported by a limited second set of data points taken using the fixed tilt V-band, X-mode antenna and fixed 61.0 GHz probe frequency at $\rho_{\rm pol} \sim 0.92$ in an L-mode upper-single-null discharge #19146, but with a triangularity

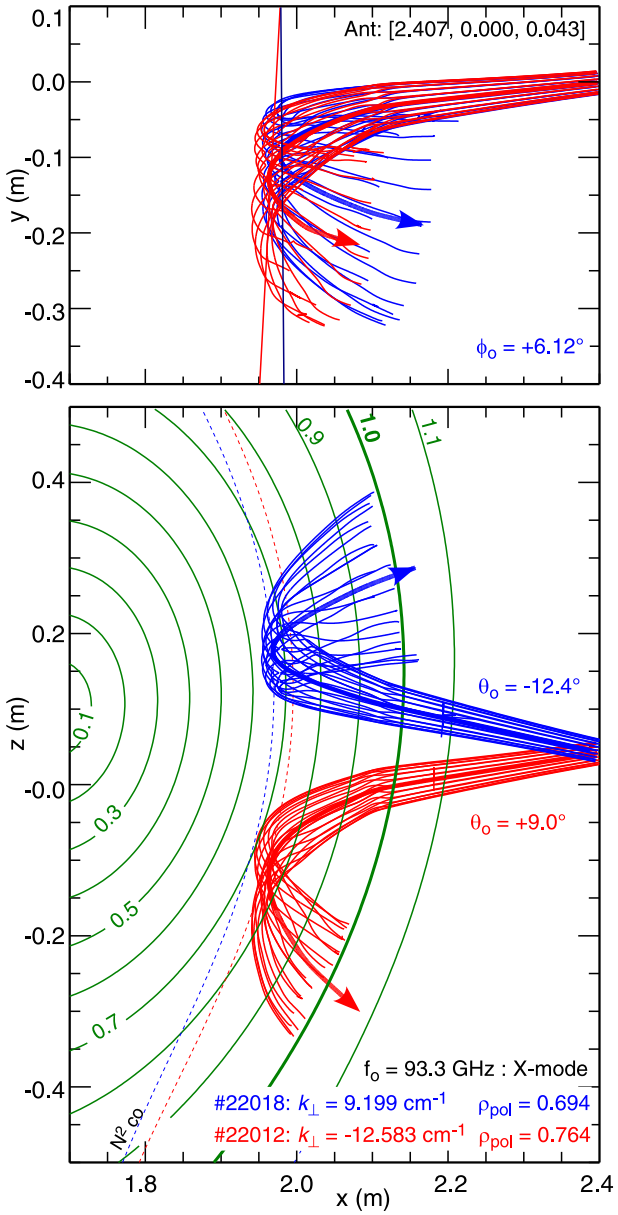

Figure 6. Torbeam traces in poloidal plane [z:x] and toroidal plane [y:x] at 93.3 GHz for AUG shot #22012 (red: $\theta_o = +9.0°$) and #22018 (blue: $\theta_o = -12.4°$). Flux surfaces contours are green solid and the respecive X-mode cutoff surfaces are red and blue lines.

scan allowing a small scan in $k_\perp = 6-9$ cm^{-1} [24, 25]. These are shown as black points in figure 7. The similarity of the spectral decay, in the limited overlap range, is surprising considering the rather different plasma parameters ($B_\mathrm{t} = -1.3$ T, $I_\mathrm{p} = +0.8$ MA, $n_\mathrm{eo} \approx 4.1 \times 10^{19}$ m^{-3}, $q_{95} \sim 3,2$ and 1.3 MW NBI heating) and suggests that the turbulence structure is rather robust in the poloidal plane of the tokamak low-field-side.

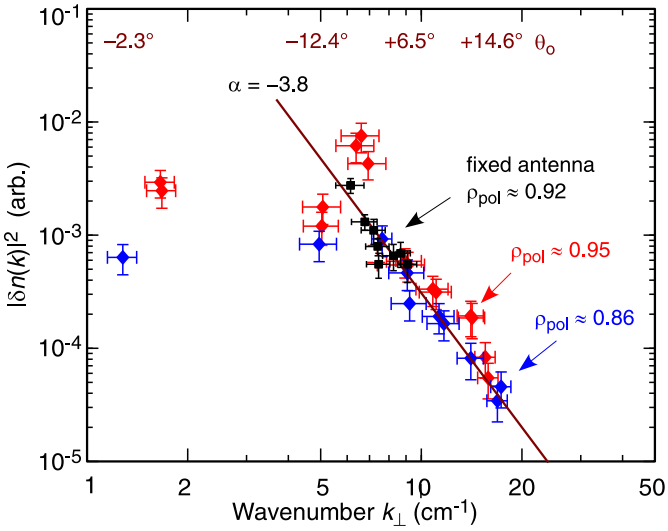

Figure 7. Experimental $k_\perp$-spectra for two radial positions: $\rho_{\rm pol} \sim 0.86$ (blue) and 0.95 (red). The corresponding antenna tilt angles θ_o are indicated along the top. The black data points are from #19146 with fixed tilt antenna at 61 GHz X-mode. An indicative fit line for $\alpha = -3.8$ is included.

4. GENE turbulence simulations

In the remainder of the paper, the measurements detailed above are compared with a numerical simulation data based synthetic diagnostic. A considerable part of this effort is dedicated to generating the physically consistent turbulence fields, which are discussed in this section. The tool employed here is the gyrokinetic plasma turbulence code GENE [26, 27] which is a physically comprehensive, hyperscalable Vlasov code that supports both local (flux-tube) and global (full-torus) calculations. However, as the latter can be quite computationally demanding, a local flux tube around $\rho_{\rm tor} = 0.8$ (toroidal flux radius) of discharge #22009 is employed with physics inputs being interpolated from the measured background profiles.

To obtain an impression of the underlying micro-instabilities being driven at that radial position, linear simulations were performed first. Figure 8 shows the growth rates and real frequencies of the dominant modes for two simulation setups used in this work. Up to $n_0 \sim 160$ toroidal mode numbers (corresponding to $k_y\rho_s \sim 1$ in GENE's native coordinate) propagating in the ion diamagnetic drift direction (positive real frequency) can be found, representing ion temperature gradient (ITG) driven micro-instabilities. At smaller scales the real frequency changes sign and trapped electron modes (TEMs) and electron temperature gradient (ETG) driven micro-instabilities prevail.

Covering ion and electron gyroradius scales simultaneously is computationally extremely challenging, and only few examples exist worldwide. In addition, the Doppler reflectometry measurements are thought to mainly consider the ion gyroradius scales. The nonlinear turbulence simulations were hence restricted to toroidal mode numbers $n_0 \sim 7 - 441$ ($k_y\rho_s = 0.053 - 3.3$) which should be sufficient to cover

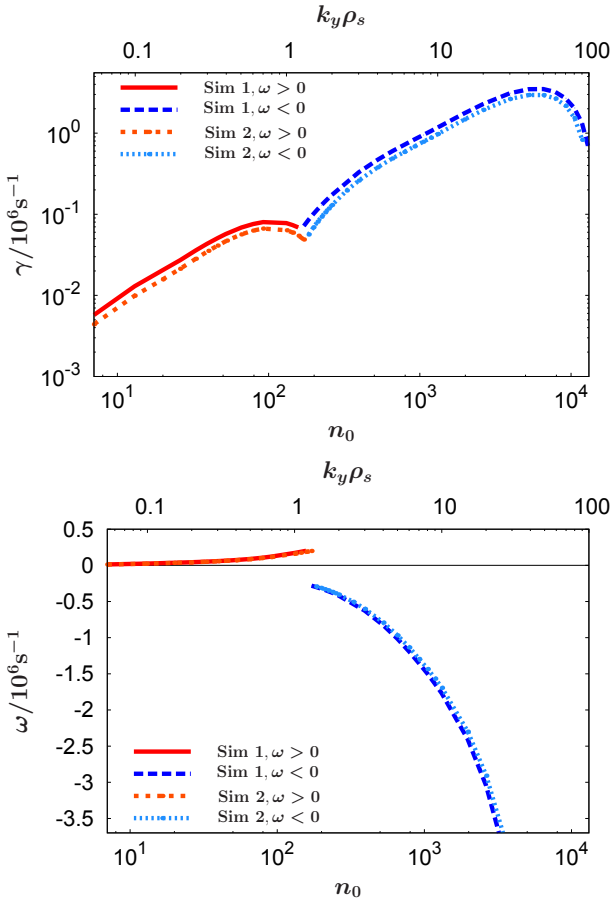

Figure 8. (Colour Online) (a) Dominant linear growth rates and (b) real frequencies from two GENE simulations for the AUG 22009 at $t = 4.1$ ms and $\rho_{\text{tor}} = 0.8$ as functions of toroidal mode number n_0 or normalized k_y wavenumber, respectively.

the turbulence features in the aforementioned scales. However, cutting at a linearly driven wavenumber may induce a spurious spectral pile-up. This effect can be counterbalanced by an artificial hyperdiffusion operator in the two perpendicular dimensions. The particular setup is one of the differences between the two simulations Sim 1 and Sim 2 used in the following analysis. The sophisticated gyro-LES methods [28] were not yet available in GENE at the time the simulations were performed and hence the hyperdiffusion amplitudes in the radial (x) and bi-normal (y) direction had to be guessed. Sim 1 used a fairly high artificial damping of $(h_x, h_y) = (0.5, 2.0)$ while Sim 2, with $(h_x, h_y) = (0.1, 0.1)$, is less constrained. Both simulations include fully gyrokinetically treated (deuterium) ions and electrons, collisions via a linearized Landau-Boltzmann operator and self-consistent electrostatic and electromagnetic fluctuations with input parameters taken from the reconstructed magnetic equilibrium and the experimental profiles.

However, with limited ion temperature measurements available, it should be noted that the ion temperature was assumed to be equal to the electron temperature. Contrary to Sim 2, the older simulation was also been performed with external parallel and

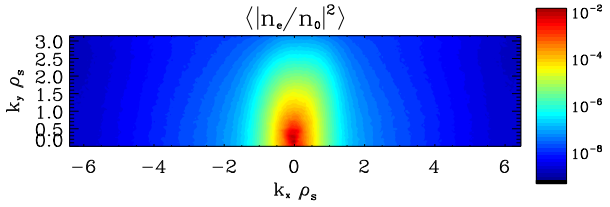

Figure 9. (Colour Online) Time-averaged electron density fluctuation spectrum from Sim 1 as function of the two wavenumbers perpendicular to the magnetic field line at $(R, z) = (2.01, -0.175)\,\mathrm{m}$.

$E \times B$ shear flow effects. In a flux tube simulation, the latter are typically implemented as discrete time-dependent jumps in k_x, which may be detrimental for a future time-dependent full-wave code interface. The spirit of the second simulation was therefore to replace this transport reduction effect by a diminished temperature gradient drive. A corresponding scan revealed that a reduction by 15 % yields the closest heat flux value as will be discussed below. Furthermore, with the experience of interfacing with simulation Sim 1 in mind, Sim 2 used a more than twice as large radial box size ($l_{x,2} \approx 276\,\rho_s$ with 512 grid points compared to $l_{x,1} \approx 125\,\rho_s$ with 256 grid points) and an updated geometry interface. On the other hand, both simulations employ the same number of grid points $(n_{ky}, n_z, n_{v\parallel}, n_\mu) = (64, 24, 32, 16)$ in the y direction, parallel along the magnetic field (z), in the parallel velocity ($v_\parallel$) and in the magnetic moment (μ) grid. The ranges of latter two coordinates are given by $-3v_{th,j} \leq v_\parallel \leq v_{th,j}$ and $\mu \leq 9T_{0j}/B_0$ where $v_{th,j} = \sqrt{2T_{0j}/m_j}$ is the thermal velocity of species j, T_{0j} its temperature, m_j its mass and $B_0 = 2.424\,\mathrm{T}$ is the reference magnetic field.

A first assessment on the validity of a gyrokinetic turbulence simulation is often based on the transport levels. At $t = 4.1\,\mathrm{ms}$ a total heating power of $P = 2.91\,\mathrm{MW}$ had been deposited in AUG shot 22009. In the radial range of interest around $\rho_{\mathrm{tor}} = 0.8$, the simulated heat flux should be slightly below this value. The simulation with nominal values (Sim 1) is already quite close. Here, $2.23 \pm 0.32\,\mathrm{MW}$ are found in the ion and $0.87 \pm 0.13\,\mathrm{MW}$ in the electron heat channel, therefore adding up to a total heat transfer rate of $3.1 \pm 0.45\,\mathrm{MW}$. The second simulation (without shear flow effects but with logarithmic temperature gradients reduced by 15 % to $-\partial/\partial\rho_{\mathrm{tor}} \ln T = 2.79$) yields a total heat flux of $2.14 \pm 0.05\,\mathrm{MW}$ with an ion heat channel contribution of about 70 % as before. This is the best match in series of gradient scans involving reductions by $5, 10, 20$ and 50 % where the first two are found significantly above the maximum deposited heating power. The latter two consistently exhibit smaller values than the simulation at 15 % reduced logarithmic temperature gradient.

Before moving on to the actual observable of interest – the perpendicular wavenumber spectra – the 2D spectrum at the GENE grid position closest to the measurement position, $(R, z) = (2.01, -0.175)\,\mathrm{m}$, will be discussed first. As is observed in figure 9, the 2D spectrum is rather anisotropic. The often employed averaging over the radial wavenumbers while computing the perpendicular spectrum may hence be

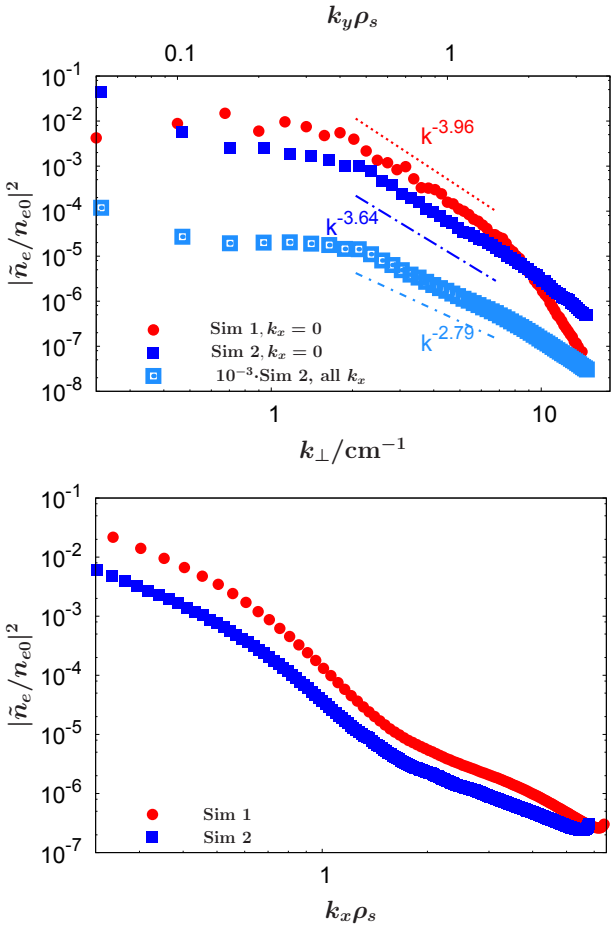

Figure 10. (Colour Online) (a) Time-averaged perpendicular and radial electron density fluctuation spectrum at $(R, z) = (2.01, -0.175)\,\mathrm{m}$ from Sim 1 and Sim 2 at $k_x = 0$. For comparison, the result averaging over all k_x modes has been added for Sim 2, but rescaled by a factor 10^{-3} for readability. Values beyond $k_\perp \sim 8\,\mathrm{cm}^{-1}$ are not taken into account for the power law fits as they are affected by the perpendicular diffusion operator. (b) Radial electron density spectrum averaged over time and k_y.

inadequate for the comparison with the Doppler reflectometry. The latter is more likely to just involve radial wavenumbers close to zero. Corresponding results for Sim 1 and 2 are shown in figure 10(a).

The qualitative behaviour is in good agreement with the experimental findings. The spectra exhibit a flat plateau followed by a 'knee' which marks the beginning of a power law $k_\perp^{-3.96}$ (Sim 1) or $k_\perp^{-3.64}$ (Sim 2), respectively. Both values are close to the Doppler reflectometry result of $k_\perp^{-3.8}$. A second, steeper spectral decay at high wavenumbers in the simulation data can be attributed to the hyperdiffusion operator which is forth order in k_y and hence translates to $\sim k_\perp^{-8}$ in the squared density fluctuations. Clearly, it is much more pronounced in Sim 1 where a much larger amplitude had been employed. A striking difference between experimental measurement and numerical study is found in the exact position of the knee, i.e. the spectral roll-over, which almost differs by one order of magnitude. A first complication in this context is given by GENE's

native coordinate k_y which is defined within the magnetic flux surface but in a non-orthogonal coordinate system while the Doppler reflectometry system is evaluating the wavenumber in a direction perpendicular to the radial and parallel coordinates. The associated conversion factor can, however, be derived from the metric coefficients [29] as follows $k_\perp = \sqrt{(g^{xx}g^{yy} - (g^{xy})^2)/g^{xx}}k_y$ and is already taken into account in the plots. The metric coefficients themselves are obtained via numerical field line tracing of the aforementioned CLISTE equilibrium. More details can be found in Refs. [29, 30]. ‡

The discrepancy is particularly mysterious given that power laws are typically linked to turbulence cascades. In a Kolmogorov-type picture the latter should form next to the injection scale which could here approximated by the ITG growth rate peak at $k_y\rho_s \sim 0.7$ or $k_\perp \sim 3\,\mathrm{cm}^{-1}$. Even this rather conservative estimate, given that the nonlinear fluxes are typically up-shifted to larger scales, would be a factor of 3 different compared to the Doppler measurement which calls for further investigations, e.g. involving full-wave scattering as described below. Furthermore, figure 10(a) includes a spectrum averaged over all radial wavenumbers for comparison. As expected and discussed before, the power law is found to be significantly different, emphasizing the need even for such lowest order synthetic diagnostics as described above. Finally, radial spectra are shown for completeness in figure 10(b). Apart from a shift in amplitude, no major difference can be seen between Sim 1 and Sim 2.

5. Full-wave simulations with IPF-FD3D

The reflectometry simulations were performed with the IPF-FD3D code [10, 14] using a two-dimensional Cartesian grid. The wave propagation is simulated from the launching antenna, to the plasma cutoff, and back to the coherent receiver, yielding the instantaneous reflectometer amplitude and phase. IPF-FD3D is a finite-difference time domain (FDTD) code [18] that simulates the propagation of electromagnetic waves in cold plasmas [20, 32] in two or three dimensions. Its main feature is the capability of simulating wave propagation in a given inhomogeneous, anisotropic (i.e. magnetized) plasma by integrating the equation of motion of the electrons:

$$\frac{\partial}{\partial t}E = \frac{1}{\varepsilon_0}\nabla \times H - \frac{1}{\varepsilon_0}J \tag{3}$$

$$\frac{\partial}{\partial t}J = \varepsilon_0\omega_{pe}^2 E - \omega_{ce}J \times \widehat{B}_0 \tag{4}$$

$$\frac{\partial}{\partial t}H = -\frac{1}{\mu_0}\nabla \times E \tag{5}$$

where $\widehat{B}_0$ is the unity vector in the direction of the background magnetic field B_0, ω_{ce} the electron cyclotron frequency, and ω_{pe} the plasma frequency. All these quantities can be time and space dependent.

‡ Note that here $k_\perp$ is not defined as $k_\perp^2 = g^{xx}k_x^2 + 2g^{xy}k_xk_y + g^{yy}k_y^2$ as is often employed in the gyrokinetics community.

The partial differential equations are translated to finite difference equations. The IPF-FD3D code implements two and three-dimensional solvers of equations (3–5) on a Cartesian Yee [16] grid. Usually it is sufficient to use 20 grid points per vacuum wavelength of the incident beam. If steep gradients, or small wavelengths are present in the plasma, this number is adjusted upwards to 200. Equations (3) and (5) for the wave E and H fields are solved with a spatial and temporal leapfrog scheme, while the electron response is integrated separately with a modified Crank-Nicolson method – which couples in to the Maxwell equations via the plasma current term J in the E field equation.

The plasma setup is given by spatial arrays of plasma density (in units of m^{-3}) and the three background field components (in units of T). They are taken from the AUG reconstructed equilibria for each experimental shot that is considered in the simulations. The density fluctuations from the GENE simulations are added on top of the equilibrium density profile, a fitted Tanh as shown in figure 4(b), with an optional scaling factor to artificially increase or decrease the fluctuation amplitude. Typical amplitudes were on the order of several percent of the background density.

For this investigation, the two-dimensional version of the code was used. The simulated domain is the poloidal plane to the magnetic field. The density fluctuation data from GENE is exported and interpolated to the $[R, z]$ plane in units of m^{-3}. A scan of the spatial resolution has shown that 18 points per vacuum wavelength is sufficient to adequately capture the plasma density features in the cases considered here. Near the cutoff, the effective resolution is larger than that because of the increased wavelength in the plasma. Simulations in 3D for thousands of turbulence fields would be prohibitively expensive in terms of CPU hours. Because of the long parallel structure sizes in fusion plasma turbulence, the problem can be treated as effectively two-dimensional. We are nevertheless exploring methods to quantify the 3D effects.

The recflectometer launching and receiving antennas are synthetic apertures at the edge of the simulation grid. The beams are fundamental Gaussians that can be modified by higher order Hermite modes so that the experimental beam geometry can be accurately modelled. The receiver samples the field at the same position and convolutes it with the complex beam pattern of the receiving antenna, which is usually the same as the launching antenna. Figure 11 shows the simulation grid, which covers the lower right portion of AUG as shown in figure 1. Overlaid on the density contour plot is the electric wave field, which is injected in the upper right edge. The many backscattered waves are seen in the lower half. In order to reduce the grid size, the vacuum between the actual antenna position and the plasma edge is not contained in the grid. Instead, the beams are injected and detected at $R = Rs$, where numerical antennas are located that correspond to the beam size and phase front curvature of the original beams at that location. An $Rs = 2.24\,\mathrm{m}$ was chosen to be just in front of the plasma edge.

For the Doppler reflectometry investigation a radial position ρ_{pol} is chosen, and the beam tracing code TORBEAM used to find the corresponding launch frequencies and their probed wavenumbers $k_\perp$ for a range of antenna tilt angles. All beams are launched into

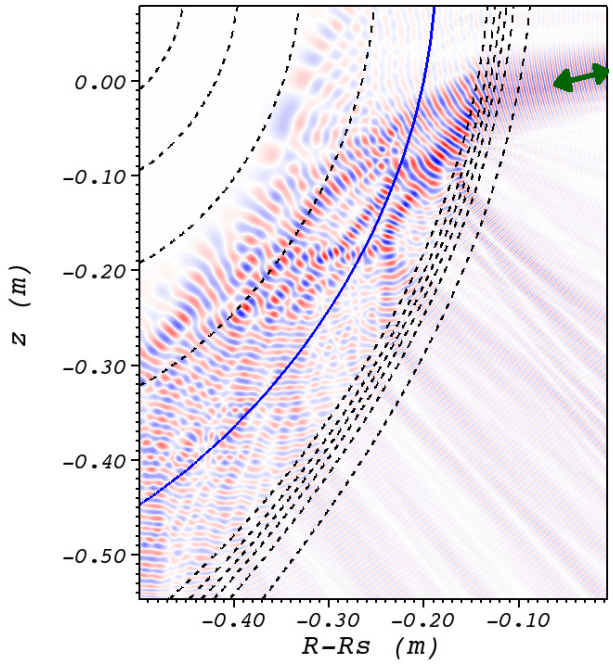

Figure 11. (Colour Online): Setup of the simulation grid for AUG. Contour plot of the density with peak at $5.87 \times 10^{19}\,\mathrm{m}^{-3}$. Solid blue contour is cutoff density at $\rho_{\mathrm{pol}} = 0.86$. The electric wave field is shown in red and blue. The beam is injected and detected at the upper right edge at an angle of 11.5° downwards (green arrow). *Rs* is the position of the source plane.

the simulation grid simultaneously. They are discriminated by their different frequencies, with the relative cross talk between beams below 10^{-10}.

6. Full-wave results

6.1. Comparison of Doppler Spectra

The expected scaling of the scattered power (in the limit of small density fluctuation amplitudes) is with the square of the turbulence strength (fluctuation power). Figure 12 shows the returned power in X-mode polarization for a resonant density perturbation at a large wavenumber. The perturbation spectrum is very narrow around the probed wavenumber. The linear dependence of received power over fluctuation power holds true over at least 7 orders of magnitude. Non-linear saturation only sets-in when the perturbation density is several percent of the cutoff density.

The fullwave simulation result using GENE Sim 1 as input is shown in figure 13. A relatively good agreement is seen in the spectral index α, between experiment and fullwave. The kink in the GENE spectrum at $k_\perp \rho_s = 0.8$ comes from the diffusion operator discussed above. Unfortunately this diffusion steepens the the spectrum considerably in the region where the spectral index was probed by the reflectometer. This had not been expected before and was then the motivation for the case Sim 2. The GENE spectrum of Sim 1 therefore does not represent the actual turbulence seen

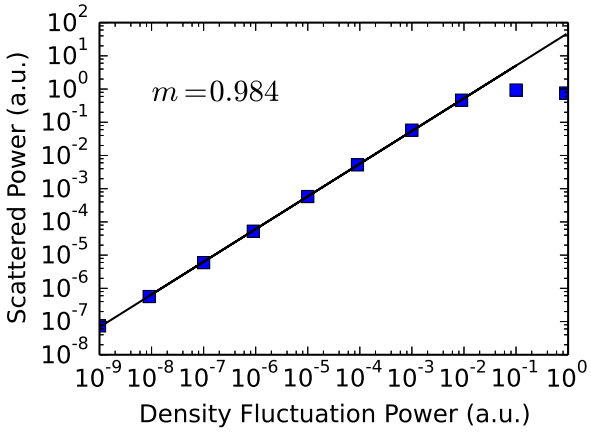

Figure 12. Ratio of scattered power to density fluctuation power. The relationship is linear ($m \approx 1$ over a wide range of fluctuation strengths, until the density fluctuation amplitude reaches about 3 % of the cutoff density.

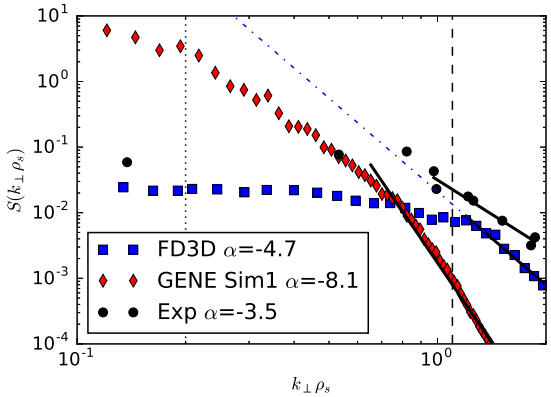

Figure 13. (Colour Online) Experimental, GENE, and fullwave (FD3D) wavenumber spectra and fits of the spectral index α for case Sim 1. Density fluctuation power is shown for GENE, and scattered microwave power for the others. The dotted line is the GENE knee position, and the dashed line is the fullwave and experimental knee position.

by experiment and the similar indices of GENE in the unaffected region and experiment are coincidental. Furthermore, no meaningful insight can be gained from the difference in the knee position between fullwave simulation and experiment. In any case, the instrument response function of the Doppler reflectometer makes the spectral index much more shallow (from -8.1 to -4.7).

However, the physical knee position is unaffected by the diffusion. It is at a much lower $k_\perp \rho_s$ in GENE (dotted line, as expected for ITG) than for both the experimental and fullwave spectra (dashed vertical line), where the transition for both is around $k_\perp \rho_s = 1.0$. Referring to figure 12, it is likely that the fullwave simulation is non-linearly saturated at a level of about 2×10^{-2}. Like a clipping amplifier, the top part of

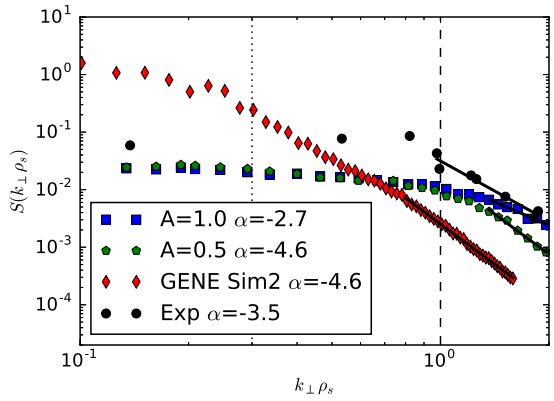

Figure 14. (Colour Online) Experimental, GENE, and fullwave (FD3D) wavenumber spectra and fits of the spectral index α for case Sim 2. Density fluctuation power is shown for GENE, and scattered microwave power for the others. A is the scaling factor of the density fluctuations in the fullwave (FD3D) simulations. The dotted line is the GENE knee position, and the dashed line is the fullwave and experimental knee position.

the spectrum shape is cut off, and the high wavenumber region with its lower density fluctuation amplitude is compressed. The observed knee in the fullwave spectrum appears at the wavenumber where the spectrum transitions from the saturated to the merely compressed region. The compression effects the shallow roll-off in the fullwave spectrum ($\alpha = -4.5$ compared to the -8.1 of the underlying fluctuations). This effect is studied in more detail in the next section.

Indeed, extrapolating $S \sim k^{-4.5}$ (blue dot-dash line) down to the GENE knee position yields a returned power of more than the input beam power already at around $k_\perp \rho_s \approx 0.4$.

The fullwave results for the GENE case Sim 2 are shown in figure 14. The wavenumbers of interest for the spectral index are again affected by the diffusion operator in GENE. However, the modification of the spectrum is less severe (α changing from -3.6 to -4.6). This means that the fullwave spectral index should be made less steep accordingly, before comparing to the experimental value. For the position of the knee, the same arguments hold as for the case of Sim 1.

Also shown is the result of scaling the turbulence by $A = 0.5$ before adding to the background density and performing the fullwave simulation. It shows the same saturation for $k_\perp \rho_s < 1$, but the spectral index is much steeper. This is interpreted as the effect of less compression for $k_\perp \rho_s > 1$ due to the lower fluctuation amplitude. It is known from earlier results [10] that the sensitivity of the Doppler reflectometer decreases as $k_\perp$ increases. The full linear fullwave spectrum would therefore be expected to be somewhat steeper than the underlying GENE spectrum.

The total fluctuation amplitude of Sim 2 was somewhat larger in the scattering region than in Sim 1, which means that the Sim 2 fluctuations should be scaled by

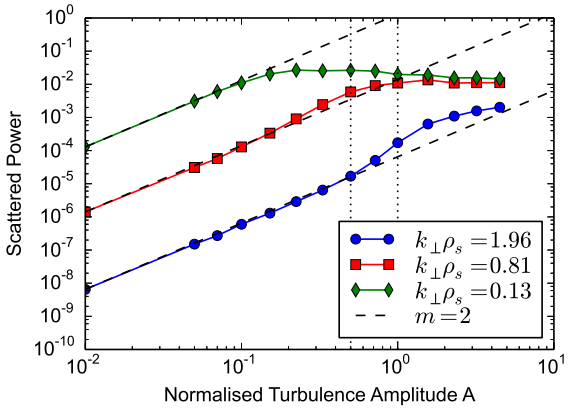

Figure 15. (Colour Online) Scaling of the scattered power with turbulent amplitude at different probed wavenumbers for synthetic turbulence. The $m = 2$ line shows the linear scaling (scattered power $\propto A^2$). The turbulence amplitude $A = 1$ corresponds to the amplitude of the GENE turbulence of Sim 2, which is 2.4 %.

$A \approx 0.77$ to get the same level of non-linearity in the fullwave simulation. Taking the average of the 2 fullwave spectra, a spectral index of around $\alpha = -3.6$ can be estimated. A fullwave simulation for $A = 0.77$ yields $\alpha = -3.5$ – which is the experimental index within errors. However, since the turbulence input was steepened at large wavenumbers by the hyperdiffusion in GENE (from $\alpha = -3.6$ to -4.6), the fullwave α should also be steeper than the experimental value by a similar amount. Therefore, the corresponding value of α in the fullwave simulation should be about $\alpha = -4.6$, assuming that the relationship between reality and experimental Doppler result is the same as the relationship between GENE and fullwave. This hints at a rather large fluctuation amplitude correction factor of $A = 0.5$, for which the actual GENE α is recovered.

In general, the steepness of the spectrum (the absolute value of α) is underestimated in X-mode at the turbulence levels present in the discharges considered. Given the error in fitting a line to limited points, the agreement is still good.

6.2. Analysis of Non-Linear Behaviour

The non-linear effect is shown in figure 15 for isotropic synthetic turbulence with a similar wavenumber spectrum as the GENE results. The three wavenumbers shown cover the whole Doppler range in X-mode. The difference to figure 12 is that a full turbulent spectrum was used here. The difference to the GENE turbulence is the isotropy in the perpendicular and radial directions. The x axis (normalized turbulence amplitude) is relative to the density fluctuation amplitude of Sim 2.

In the limit of small density fluctuation strength, the ideal 'linear' scaling is seen, where the scattered power is proportional to the square of the density perturbation amplitude. For the low wavenumber ($k_\perp\rho_s = 0.13$, green diamonds), a saturation point

is reached at normalized turbulence amplitude of $A_{sat} \approx 0.1$, after which the scattered power remains constant and even declines for $A > 1$. The intermediate wavenumber ($k_\perp \rho_s = 0.81$, red squares) shows the same saturation behaviour. It is shifted by a factor of 10 to larger $A_{sat} \approx 1$, corresponding to its hundredfold lower spectral power (which can be seen in the plot for $A = 10^{-2}$). The analogous behaviour is seen in the high wavenumber case ($k_\perp \rho_s = 1.96$, blue circles), again shifted down and to the right appropriately.

An important new phenomenon is observed for the intermediate and high wavenumbers: A super-linear enhancement of the scattered power for $A < A_{sat}$ This effect is also reported in [33], where both a physical optics code and a fullwave code showed a very similar effect. Together with the saturation effect, this can drastically modify the shape of the scattered power spectrum.

The dotted $A = 1$ line in figure 15 corresponds to the nominal turbulence strength in Sim 2. This means that for $k_\perp \rho_s$ between 0.13 and 0.81, the wavenumber spectrum seen through Doppler reflectometry should be nearly flat, because the $k_\perp \rho_s = 0.13$ and $k_\perp \rho_s = 0.81$ graphs have nearly the same value. Indeed, this is seen in figure 14 (blue squares). The steepness of the underlying GENE spectrum is drastically reduced because of this saturation effect which squishes down on the low $k_\perp$, high fluctuation strength part of the spectrum.

Conversely, the range from $k_\perp \rho_s = 0.81$ to $k_\perp \rho_s = 1.96$ is in the linear region at its low-$k_\perp$ end, and in the enhancement region towards its high-$k_\perp$ end. This should again have the effect of decreasing the steepness of the underlying GENE spectrum, which again is observed in figure 14 (blue squares): a spectral index of -2.7 is seen instead of -4.6 (GENE).

Furthermore, any 'knee' observed in the Doppler derived spectrum is merely caused by the saturation effect, and may not be interpreted as the scale of the turbulent drive.

Repeating this procedure for $A = 0.5$, we expect from figure 15 and see in figure 14 (green pentagons) the saturation effect on the $k_\perp \rho_s < 0.81$ side. However, since now the high-$k_\perp$ end of the spectrum is in the linear region, this part of the spectrum is not modified very much and we get the same spectral index both for GENE and the fullwave result.

In summary, the fullwave simulations of the Doppler reflectometer instrument response function have explained the difference between the density fluctuation wavenumber spectra seen in the plasma turbulence simulation, and the ones derived from Doppler reflectometry. In X-mode polarization, the non-linear saturation at small wavenumbers creates a bogus 'knee' in the spectrum, whereas non-linear enhancement makes the roll-off at large wavenumbers less steep than expected. While in principle, the fullwave derived spectra should have exactly the shape observed in experiment, a discrepancy in the spectral index was present, which could be resolved by artificially decreasing the fluctuation strength of the turbulence provided by GENE by a factor of 0.5. This large decrease cannot be fully motivated by uncertainties in the GENE inputs. Given the sensitivity of the gyrokinetic simulations on the experimentally determined profiles,

future attempts with improved diagnostics may yield better agreement. However, the large decrease may here also be linked to the particular assumptions that had to be made. Especially in Sim 2, where the $E \times B$ shear mechanism was turned off and temperature gradients were adjusted to still bear the same heat fluxes as in the experiment, it is possible that the resulting fluxes were achieved by a change both in fluctuation amplitude and density-temperature cross phases. This would mean that the resulting fluctuations were not fully representative of the true physical causes for the heat fluxes. However, it is not clear if this can account for the factor of 0.5 in the density fluctuation amplitude.

7. Conclusions

This paper presents results from a fullwave synthetic diagnostic for Doppler reflectometry on the tokamak ASDEX Upgrade. It is a first attempt to make a detailed comparison of fullwave and gyrokinetic turbulence based synthetic Doppler reflectometry signals with experimental measurements. Several areas of improvement were identified and in some cases implemented. These include the need for accurate temperature gradient measurements, the treatment of $E \times B$ shear and the dissipation of high wavenumber fluctuations in the turbulence simulations, as well as the treatment of the plasma motion inside the fullwave simulations.

Considerable effort was undertaken to first get a full picture of the micro-turbulence in the relevant spatial scales. Extensive simulations with the gyrokinetic plasma turbulence code GENE were performed to ensure a realistic simulation. The resulting turbulence fields were used as input to the wave propagation code IPF-FD3D which uses a finite difference time domain method to model the X-mode Doppler reflectometer diagnostic in AUG.

Significant differences have been observed between the experimental results for the perpendicular wavenumber spectrum of the density fluctuations and the direct spectra obtained from the turbulence simulation. Especially the position of the 'knee' was shifted to higher wavenumbers, which contradicts the interpretation of the knee as the turbulent drive scale.

It was possible to explain this in terms of a non-linear instrument response function of the Doppler reflectometer. At the given fluctuation strengths, low to medium wavenumbers saturate the reflectometer signal, while scattering at high wavenumbers is enhanced. This creates a pseudo-knee in the Doppler derived spectrum, while the actual knee is lost in the saturated part of the spectrum. This important result stresses the need for an accurate model or simulation of the diagnostic.

The steepness of the spectrum at high wavenumbers (spectral index) is also affected by the non-linear scaling. However, the steepness is systematically underestimated when comparing the fullwave result to the experimental spectra. A strong sensitivity to the absolute fluctuation strength was found. The spectral indices could be reconciled by artificially reducing the turbulence amplitude, which points to an overestimation of the turbulence amplitude by GENE. On the other hand, the required factor of 0.5 in the

amplitude is quite large, given that the unscaled GENE results do match the overall heat flux reasonably well. With the given uncertainties in the gradients and heat flux and the strong sensitivity of the gyrokinetic results with respect to these in mind, the need for more precise data both from the experimental measurements as well as further parameter scans in the gyrokinetic code is obvious.

While the fullwave simulations, in concert with the plasma turbulence simulations, have not yielded a 100 % agreement of the spectra and their spectral indices, the result is still robust, and the non-linear scaling serves as a good model to understand the instrument response function. In further investigations, the position of the pseudo-knee compared to the known ITG scale (and also using an assumed spectrum) could be used to gauge the absolute turbulence level from the Doppler data alone, without doing costly turbulence and fullwave simulations.

Only one scenario of Doppler reflectometry has been investigated here, probing a typical ASDEX Upgrade L mode plasma at a radial position $\rho_{\mathrm{pol}} = 0.86$, which is inside the pedestal region with a shallow density gradient at a density fluctuation level of 2.4 %. We expect the saturation effect in X mode to be a factor also in other scenarios, but simulations must first be made to gauge its strength. For example, in the large gradient region near the edge, the effect could be reduced, as suggested by the short gradient length case in [10]. On the other hand, the relative density fluctuation amplitude is larger in the edge region, which would enhance the effect. A small "library" of fullwave simulations for various tokamak scenarios and probing positions should be compiled to support the Doppler reflectometer analysis.

The results presented in this paper are therefore encouraging, but there is a need for better experimental data and for measurements in O-mode polarization. This data has become available and has been published [34]. In addition, a more in-depth analysis of the non-linear scaling is planned for both X and O-mode.

Acknowledgments

The simulations were performed on the HPC-FF computer cluster in Jülich, Germany; on the BOB linux cluster at RZG; on hornet and hazelhen at HLRS Stuttgart; on bwUniCluster funded by the Ministry of Science, Research and Arts and the Universities of the State of Baden-Württemberg, Germany, within the framework programme bwHPC.

This work was also partly performed within the framework of the Helmholtz Virtual Institute on Plasma Dynamical Processes and Turbulence Studies using Advanced Microwave Diagnostics.

References

[1] Conway G.D. 2006 Microwave reflectometry for fusion plasma diagnosis *Nucl. Fusion* **46** S665–S669
[2] Sabot R., Clairet F., Honoré C., Bottereau C., Chareau J.-M., GabilletF., Hennequin P., Heuraux S., Leclert G., Sirinelli A., Truc A., and Vermare L. 2004 Advances of reflectometry

on tore-supra: From edge density profile to core density fluctuations *Intnl. J. Infrared and Millimeter Waves* **25** 229–246

[3] Holzhauer E., Hirsch M., Grossmann T., Branas B., and Serra F. 1998 Theoretical and experimental investigation of the phase-runaway in microwave reflectometry *Plasma Phys. Control. Fusion* **40** 1869–1886

[4] Hirsch M., Holzhauer E., Baldzuhn J., Kurzan B., and Scott B. 2001 Doppler reflectometry for the investigation of propagating density perturbations *Plasma Phys. Control. Fusion* **43** 1641–1660

[5] Hirsch M. and Holzhauer E. 2004 Doppler reflectometry with optimized temporal resolution for the measurement of turbulence and its propagation velocity *Plasma Phys. Control. Fusion* **46** 593–609

[6] Conway G.D., Poli E., Happel T., and the ASDEX Upgrade Team 2010 Interaction of mean and oscillating plasma flows across confinement mode transitions *Plasma Fus. Res.* **5** S2005–S2005

[7] Conway G.D., Schirmer J., Klenge S., Suttrop W., Holzhauer E., and the ASDEX Upgrade Team 2004 Plasma rotation profile measurements using Doppler reflectometry *Plasma Phys. Control. Fusion* **46** 951–970

[8] Hennequin P., Sabot R., Honoré C., Hoang G.T., Garbet X., Truc A., Fenzi C., and Quéméneur A. 2004 Scaling laws of density fluctuations at high k on tore supra *Plasma Phys. Control. Fusion* **46** B121 doi:10.1088/0741-3335/46/12B/011

[9] Schirmer J., Conway G.D., Holzhauer E., Suttrop W., Zohm H., and the ASDEX Upgrade Team 2007 Radial correlation length measurements on ASDEX Upgrade using correlation Doppler reflectometry *Plasma Phys. Control. Fusion* **49** 1019–1039

[10] Lechte C. 2009 Investigation of the Scattering Efficiency in Doppler Reflectometry by Two-Dimensional Full-Wave Simulations *IEEE Trans. Plasma Sci.* **37** 2009

[11] U. Stroth, A. Banon Navarro, G.D. Conway, T. Görler, T. Happel, P. Hennequin, C. Lechte, P. Manz, P. Simon, A. Biancalani, E. Blanco, C. Bottereau, F. Clairet, S. Coda, T. Eibert, T. Estrada, A. Fasoli, L. Guimarais, Ö. Gürcan, Z. Huang, F. Jenko, W. Kasparek, C. Koenen, A. Krämer-Flecken, M.E. Manso, A. Medvedeva, D. Molina, V. Nikolaeva, B. Plaum, L. Porte, D. Prisiazhniuk, T. Ribeiro, B.D. Scott, U. Siart, A. Storelli, L. Vermare, and S. Wolf. Experimental turbulence studies for gyro-kinetic code validation using advanced microwave diagnostics. *Nuclear Fusion*, 55(8):083027, 2015.

[12] J. C. Hillesheim, C. Holland, L. Schmitz, S. Kubota, T. L. Rhodes, and T. A. Carter. 2D full wave modeling for a synthetic doppler backscattering diagnostic *Rev. Sci. Instrum.* **83** 10E331, 2012

[13] E. Blanco and T. Estrada. 2008 Study of Doppler reflectometry capability to determine the perpendicular velocity and the k-spectrum of the density fluctuations using a 2D full-wave code *Plasma Phys. Control. Fusion* **50** 095011

[14] Lechte C., Holzhauer E., Stroth U, and Conway G.D 2007 Full-Wave Doppler Reflectometry Simulations in 2D *Proc. 8th International Reflectometer Workshop, St.Petersburg, Russia*

[15] Gusakov E.Z. and Surkov A.V. 2004 Spatial and wavenumber resolution of Doppler reflectometry *Plasma Phys. Control. Fusion* **46** 1143–1162

[16] Yee K.S. 1966 Numerical solution of initial boundary value problems involving Maxwell's equations in isotropic media *IEEE Trans. Antennas and Propagation* **14** 302–307

[17] Kron C. 1971 *Diakoptics and Networks* (Academic Press, New York)

[18] Taflove A. and Hagness S.C. 2000 *Computational Electrodynamics* (Artech House, Norwood, MA 02062)

[19] Holzhauer E. and Rohrbach G. 1992 *Proc. 1st IAEA Techn. Comm. Meeting on Microwave Reflectometry on Fusion Plasma Diagnostics (Abingdon 1992)*, page 133. (IAEA)

[20] Young J.-L. 1994 A full finite difference time domain implementation for radio wave propagation in a plasma *Radio Science* **29** 1513–1522

[21] Kolmogorov A.N. 1991 The local structure of turbulence in incompressible viscous fluid for very large reynolds number *Dokl. Akad. Nauk. SSSR* **30** 9–13 (1941), reprinted in *Proc. Roy. Soc. London A* 434 (1991)

[22] Kraichnan R.H. 1967 Inertial ranges in two-dimensional turbulence *Phys. of Fluids* **10** 1417
[23] Tröster C. 2008 *Development of a flexible Doppler reflectometry system and its application to turbulence characterization in the ASDEX Upgrade tokamak* PhD thesis, Ludwig-Maximilians-Universität, München
[24] Conway G.D., Tröster C., Schirmer J., Suttrop W., Lechte C., Holzhauer E., Scott B., Poli E., Zohm H. and the ASDEX Upgrade team 2008 Turbulence and geodesic acoustic mode behavioural studies in ASDEX Upgrade using Doppler reflectometry *Proc. IAEA-CN-165/EX/P5-38* (IAEA, Vienna)
[25] Conway G.D., Tröster C., Schirmer J., Lechte C., Suttrop W., Poli E., Zohm H. and the ASDEX Upgrade team 2009 Turbulence measurements using Doppler reflectometry on ASDEX Upgrade *Proc. 9th Intl. Reflectometer Workshop - IRW9 (Lisbon)*, May 2009, http://www.ipfn.ist.utl.pt/irw9/proceedings.html
[26] Jenko F., Dorland W., Kotschenreuther M., and Rogers B.N. 2000 Electron temperature gradient driven turbulence *Phys. Plasmas* **7** 1904
[27] Görler T., Lapillonne X., Brunner S., Dannert T., Jenko J., Merz F., and Told D. 2011 The global version of the gyrokinetic turbulence code GENE *J. Comput. Phys.* **230** 7053–7071
[28] Bañón Navarro A., Teaca B., Jenko F., Hammett G.W., and Happel T. 2014 Applications of large eddy simulation methods to gyrokinetic turbulence *Phys. Plasmas* **21** 032304
[29] Told D. 2012 *Gyrokinetic Microturbulence in Transport Barriers* PhD thesis, Universität Ulm, Germany
[30] P. Xanthopoulos and F. Jenko. 2006 Clebsch-type coordinates for nonlinear gyrokinetics in generic toroidal configurations. *Phys. Plasmas* **13** 092301
[31] Note that here $k_\perp$ is not defined as $k_\perp^2 = g^{xx}k_x^2 + 2g^{xy}k_xk_y + g^{yy}k_y^2$ as often employed in the gyrokinetics community.
[32] Lijun Xu and Naichang Yuan. 2006 FDTD formulations for scattering from 3-D anisotropic magnetized plasma objects *IEEE Antennas and Wireless Propagation Lett.* **5** 335–338
[33] J. R. Pinzón, T. Happel, E. Blanco, G. D. Conway, T. Estrada, U. Stroth. 2017 Enhanced Doppler reflectometry power response: physical optics and 2D full wave modelling *Plasma Phys. Control. Fusion* **59** 035005 http://dx.doi.org/10.1088/1361-6587/aa543c
[34] T. Happel, T. Görler, C. Lechte, M. Bernert, G.D. Conway, S. J. Freethy, P. Hennequin, C. Honoré, J. Pinzón, U. Stroth, and the ASDEX Upgrade Team. 2017 Comparison of detailed experimental wavenumber spectra with gyrokinetic simulation aided by two-dimensional full-wave simulations. *Plasma Phys. Control. Fusion* https://doi.org/10.1088/1361-6587/aa645b